



Dirac fermions on wires confined to the graphene Möbius stripL. N. Monteiro  and C. A. S. Almeida *Universidade Federal do Ceará (UFC), Departamento de Física, Campus do Pici, 60455-760 Fortaleza, Ceará, Brazil*

J. E. G. Silva

Universidade Federal do Cariri (UFCA), Cidade Universitária, 63048-080 Juazeiro do Norte, Ceará, Brazil

(Received 2 April 2023; revised 17 September 2023; accepted 20 September 2023; published 29 September 2023)

We investigate the effects of the curved geometry on a massless relativistic electron constrained to a graphene strip with a Möbius strip shape. The anisotropic and parity violating geometry of the Möbius band produces a geometric potential that inherits these features. By considering wires along the strip width and the strip length, we find exact solutions for the Dirac equation and the effects of the geometric potential on the electron were explored. In both cases, the geometric potential yields to a geometric phase on the wave function. Along the strip width, the density of states depends on the direction chosen for the wire, a consequence of the lack of axial symmetry. Moreover, the breaking of the parity symmetry enables the electronic states to be concentrated on the inner or on the outer portion of the strip. For wires along the strip length, the nontrivial topology influences the eigenfunctions by modifying their periodicity. It turns out that the ground state has a period of 4π whereas the first excited state is a 2π periodic function. Moreover, we found that the energy levels are half-integer multiples of the energy of the ground state.

DOI: [10.1103/PhysRevB.108.115436](https://doi.org/10.1103/PhysRevB.108.115436)**I. INTRODUCTION**

Since its discover, graphene has startled researchers due to its outstanding electronic, mechanical, and thermal properties [1,2]. This single-layer sheet of carbon exhibits high carrier mobility (vanishing effective electron mass) [3] and thus, the electron is described as a massless chiral Dirac fermion on a flat surface [4]. As a result, graphene offers a bridge between condensed matter physics and quantum field theory in two dimensions [5]. Indeed, graphene produces well-known relativistic effects, such as *Zitterbewegung* [6] and the Klein paradox [7]. More recently, relativistic effects were found in Weyl semimetals [8], Majorana fermions [9], Bogoliubov particles [10], and kagome crystals [11].

By bending the two-dimensional sheet or considering the strain effects on the membrane, graphene also becomes a table-top laboratory for curved-spaces phenomena [12,13]. In fact, the curved geometry or the strain tensor modify the effective Hamiltonian leading to a position-dependent Fermi velocity [14]. Moreover, the coupling between the Dirac fermion and the curved geometry/strain provides pseudogauge fields whose effects depend on the particular geometry/strain [15–18]. Despite being two-dimensional, graphene naturally displays ripples [19,20] and corrugations [21]. These deformations of the surface significantly modify the electronic and thermal graphene properties [22]. The effects of the curved geometry on the electronic properties, the so-called *curvatronics*, has been explored in different geometries, such as the cone [23], helicoid strip [24,25], catenoid bridge [26,27], and torus [28].

Another noteworthy effect produced by the curved geometry is the so-called geometric phase [29]. The edge states [30] or the presence of defects, such as disclinations [31],

produce geometric phases modifying the electronic properties. On conical graphene surfaces, a constant geometric gauge field yields to a geometric phase depending on the conical deficit angle [32]. Furthermore, the out-of-plane deformations of the graphene layer also lead to modifications on the optical conductivity due to Aharonov-Bohm type interference [33].

Besides the curved geometry, nontrivial topology also plays a central role on the electronic features of the low-dimensional system [34]. For instance, performing a π twist on one end of a graphene ribbon and connecting one end to the other, we obtain a graphene Möbius strip [35,36]. This graphene membrane behaves as a topological insulator with stable edge states [37]. Moreover, the half twist modifies the rotational invariance of the fields and particles constrained to move along the Möbius band [38]. Several investigations on the formation [39], stability [40], charge transfer [41], magnetic properties [42], and quantum spin-Hall effect [43,44] of the graphene Möbius strip were performed. These properties are rather different from those obtained from the usual cylindrical graphene rings [45]. Indeed, the curvature of the Möbius strip modifies the energy spectrum of nonrelativistic electrons, whose isotropic and parity symmetries are broken [46]. For relativistic electrons, the influence of a flat Möbius strip was investigated by assuming nontrivial boundary conditions [47].

In this work we study the effects of the graphene Möbius strip curved geometry on effective massless relativistic electrons. Unlike some previous works that used a discrete tight-binding approach [37,39,40], we employed a continuum analysis wherein an effective massless Dirac fermion is constrained to a curved surface. Since the Dirac equation on a curved surface does not couple with the curvature

[48,49], the effects of the curved geometry stem from the spinorial connection which acts as a pseudomagnetic potential induced by the curved geometry [50]. As a result, a geometric phase determines the density of states for wires along the Möbius strip width. The breaking of the parity and isotropy symmetries yields to states localized on the inner or outer portion of the strip depending on the angle chosen for the wire. For wires along the strip length (angular direction), the geometric phase has an Aharonov-Bohm like effect, not modifying the density of states for a single electron. Nevertheless, the ground state wave function has a period of 4π , whereas the first excited state is a 2π periodic function, due to the strip twist. Furthermore, the nontrivial topology also leads to an energy spectrum given as half-integer multiples of the ground state energy. These results agree with the modified boundary conditions analysis performed in Refs. [46,47].

This work is organized as follows. In Sec. II we briefly review the main definitions and properties of the Möbius strip geometry, such as the metric, curvatures, and connection. In Sec. III, we obtain the effective Hamiltonian for the massless Dirac particle on the surface and derive the expression for the geometric potential which depends on the geometric connection. In Sec. IV we obtain the exact solutions for the electron on wires along the width and the length of the strip. The energy levels and the effects of the nontrivial topology on the states and spectrum is discussed. Finally, additional comments and perspectives are outlined in Sec. V.

II. MÖBIUS STRIP AND ITS PROPERTIES

In this section we present the coordinate system to describe the graphene Möbius strip and study its main geometric features, such as the Gaussian and the mean curvatures and the connection 1-forms.

The graphene Möbius strip is a surface constructed by joining the two ends of a graphene ribbon after twisting one end by a π rotation, as shown in Fig. 1 [35]. This surface can be described by the following coordinate system [35,46],

$$\begin{aligned} \mathbf{r}(u, \theta) &= \left(a + u \cos \frac{\theta}{2}\right) \cos \theta \hat{\mathbf{i}} + \left(a + u \cos \frac{\theta}{2}\right) \sin \theta \hat{\mathbf{j}} \\ &\quad + u \sin \frac{\theta}{2} \hat{\mathbf{k}} \\ &= \left(a + u \cos \frac{\theta}{2}\right) \hat{\mathbf{r}} + u \sin \frac{\theta}{2} \hat{\mathbf{k}}, \end{aligned} \quad (1)$$

where $2L$ is the strip width, $-L \leq u \leq L$ is a coordinate along the width, and $0 \leq \theta \leq 2\pi$ is the angular coordinate. The coordinate u is the distance between the center of the strip and its end point, as shown in Fig. 1. Furthermore, the parameter a is the radius of the central circle and the radial unit vector is $\hat{\mathbf{r}} = \cos \theta \hat{\mathbf{i}} + \sin \theta \hat{\mathbf{j}}$. A remarkable feature of the Möbius strip is its non-orientability. Indeed, performing a 2π rotation on the outer edge of the strip ($u = L$), the outer edge becomes the inner edge ($u = -L$). Throughout the work, we use $L = 1$.

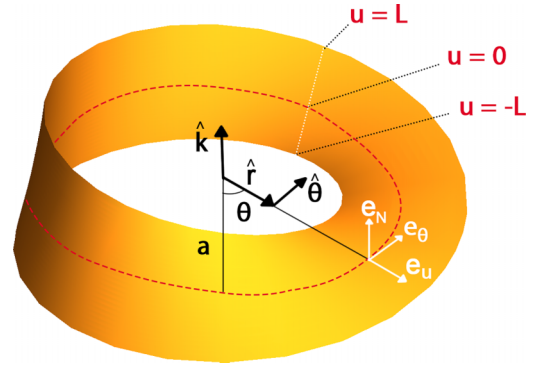


FIG. 1. Coordinates and base vectors on the Möbius strip.

The tangent vectors, defined as $e_i = \frac{\partial \mathbf{r}}{\partial x^i}$, have the form

$$e_u = \frac{\partial \mathbf{r}}{\partial u} = \cos \frac{\theta}{2} \hat{\mathbf{r}} + \sin \frac{\theta}{2} \hat{\mathbf{k}}, \quad (2)$$

$$e_\theta = \frac{\partial \mathbf{r}}{\partial \theta} = \left(a + u \cos \frac{\theta}{2}\right) \hat{\theta} - \frac{u}{2} \sin \frac{\theta}{2} \hat{\mathbf{r}} + \frac{u}{2} \cos \frac{\theta}{2} \hat{\mathbf{k}}. \quad (3)$$

From the tangent vectors, we can define the Möbius strip metric g_{ij} as

$$g_{ij} = e_i \cdot e_j = \begin{pmatrix} 1 & 0 \\ 0 & \beta^2(u, \theta) \end{pmatrix}, \quad (4)$$

where the angular metric factor β is given by [46]

$$\beta(u, \theta) = \sqrt{\frac{u^2}{4} + \left[a^2 + u \cos \left(\frac{\theta}{2}\right)\right]^2}. \quad (5)$$

In Fig. 2 we plot the angular metric function $\beta(u, \theta)$ for some values of the inner radius a with L fixed to $L = 1$. In Fig. 2(a) we choose a such that $L/a = 0.375$, i.e., $a = 2.66$, for which nanorings were obtained. As we increase the ratio L/a , as for $L/a = 1$ in Fig. 2(b) and for $L/a = 1.89$ in Fig. 2(c), the Möbius strip becomes more compact. The ratio $L/a = 1.89$ is a critical value for a Möbius strip due to mechanical properties [39].

Thus, the $2 + 1$ infinitesimal line element has the form

$$ds^2 = -dt^2 + du^2 + \beta^2(u, \theta) d\theta^2. \quad (6)$$

It is worthwhile to mention that the metric tensor for a cylinder (nanotubes) has the form shown in Eq. (6) with $\beta = a$, whereas for the conical surface (graphitic cone), $\beta = \alpha u$, where α is the so-called angular deficit [23]. Other graphene-based surfaces, such as the helicoid [24], catenoid [26,27], and torus [28], can also be described by the metric in Eq. (6).

The anisotropy of the Möbius strip breaks some surfaces symmetries, such as the parity symmetry, as we can see by $\beta(-u, -\theta) \neq \beta(u, \theta)$. However, a sort of modified Möbius parity symmetry holds, where

$$\beta(-u, 2\pi - \theta) = \beta(u, \theta). \quad (7)$$

This modified parity symmetry stems from the twist performed on the strip. In Fig. 2, we plotted the angular metric component β for $a = 1$ and $-1 \leq u \leq 1$, where the Möbius parity symmetry in Eq. (7) is shown.

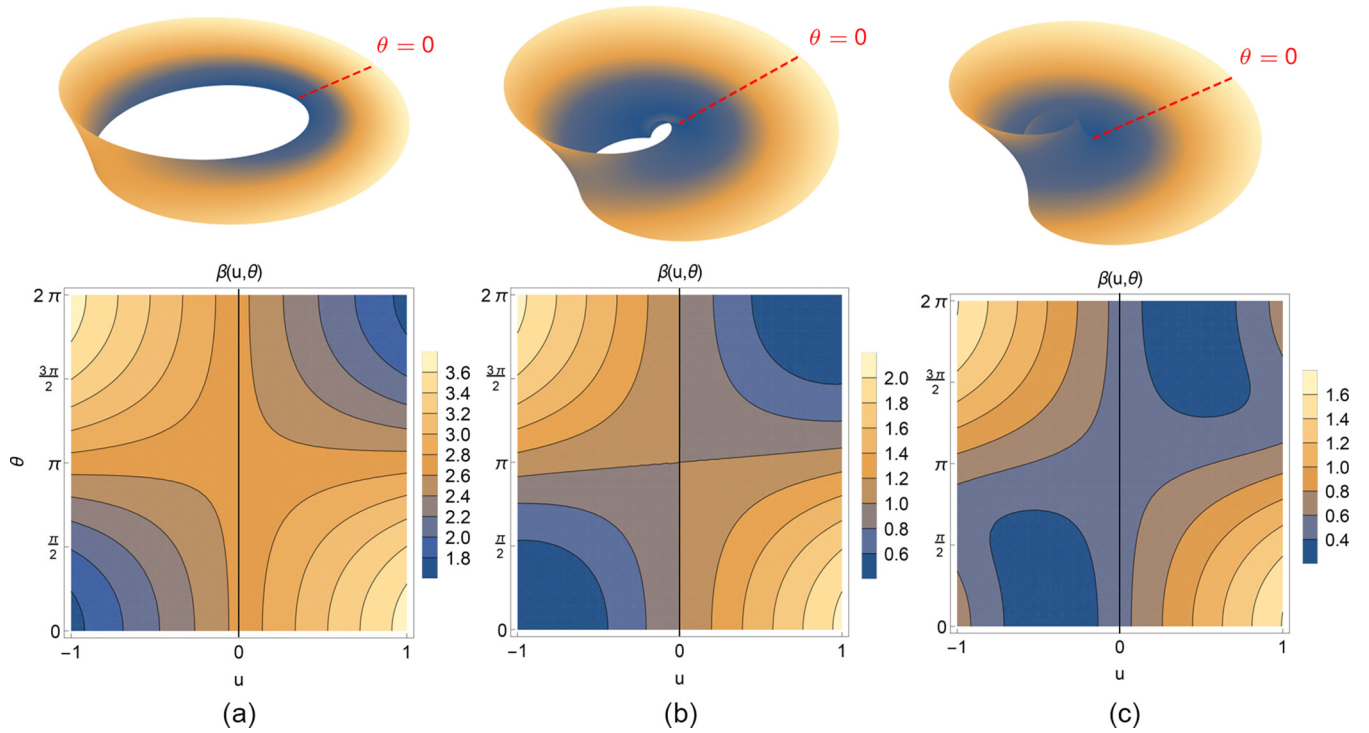


FIG. 2. Angular metric function $\beta(u, \theta)$ for $L = 1$, with $L/a = 0.375$ (a), $L/a = 1$ (b), and $L/a = 1.89$ (c), which encodes the geometrical properties of the Möbius graphene strip. The function shows a twisted parity symmetry.

The Möbius strip curvatures also exhibit the twisted parity symmetry in Eq. (7). Indeed, the expressions for the mean curvature M and the Gaussian curvature K are given by [46]

$$M = \frac{2[2(a^2 + u^2) + 4au \cos \frac{\theta}{2} + u^2 \cos \theta] \sin \frac{\theta}{2}}{[4a^2 + 3u^2 + 2u(4a \cos \frac{\theta}{2} + u \cos \theta)]^{\frac{3}{2}}} \quad (8)$$

and

$$K = -\frac{1}{\beta^2} \partial_u^2 \beta = -\frac{4a^2}{[4a^2 + u^2 + 8au \cos(\theta/2) + 4u^2 \cos^2(\theta/2)]^2}. \quad (9)$$

The behavior of the Gaussian and the mean curvatures are shown in Figs. 3 and 4, respectively. We adopt the same values for the ratio L/a as done for the β function, i.e., $L/a = 0.375$ (a), $L/a = 1$ (b), and $L/a = 1.89$ (c). Note that the curvature profiles depend on the ratio L/a . Unlike the cylindrical nanorings, where the Gaussian curvature vanishes and the mean curvature is constant, the distribution of the curvatures on the Möbius strip depends on the position u, θ and the ratio L/a .

As we will see in the next section, the massless relativistic electron couples with the surface connection instead of the curvature. Accordingly, in order to define the fermion dynamics on the surface, we have to adopt the so-called *vielbein* formalism [13]. Indeed, consider a set of matrices e_μ^a such that [23]

$$g_{\mu\nu} = e_\mu^a e_\nu^b \eta_{ab}. \quad (10)$$

In (2 + 1) dimensions, the matrices e_μ^a are $SO(1, 2)$ invariant and they are called *dreibeins*. Using the *dreibeins* we can define a local moving co-frame as $e^a = e_\mu^a dx^\mu$. For the

Möbius metric in Eq. (6), the moving co-frame has the form

$$\begin{aligned} e^0 &= dt, \\ e^1 &= \cos \theta du - \beta \sin \theta d\theta, \\ e^2 &= \sin \theta du + \beta \cos \theta d\theta. \end{aligned} \quad (11)$$

The presence of the trigonometric functions in Eq. (11) reveals the local rotational invariance on the surface. Using the torsion-free condition, $de^a + \omega_b^a \wedge e^b = 0$, the only nonvanishing connection 1-form $\omega_b^a = \Gamma_{b\mu}^a dx^\mu$ is given by

$$\omega_2^1 = -(\partial_u \beta - 1)d\theta. \quad (12)$$

Note that for a conical graphitic surface, $\beta = \alpha u$, and then, $\omega_2^1 = -(\alpha - 1)d\theta$ [23].

III. FERMIONS COUPLED TO THE MÖBIUS STRIP

Once we have reviewed the main geometric features of the graphene Möbius strip, in this section we describe how the effective massless electron couples to the graphene Möbius strip. We study the electron properties in the continuum limit, where the electron dynamics is governed by a Dirac equation defined on the curved graphene strip [13]. The curved geometry induces a pseudomagnetic-potential vector Γ_μ , known as the spinorial connection. Then, we explore some features and effects of the spinorial connection, such as the geometric potential.

We employ the intrinsic coupling of the electron to the curved surface, wherein the massless Dirac equation on the surface is given by [13]

$$i\hbar\gamma^\mu D_\mu \psi = 0. \quad (13)$$

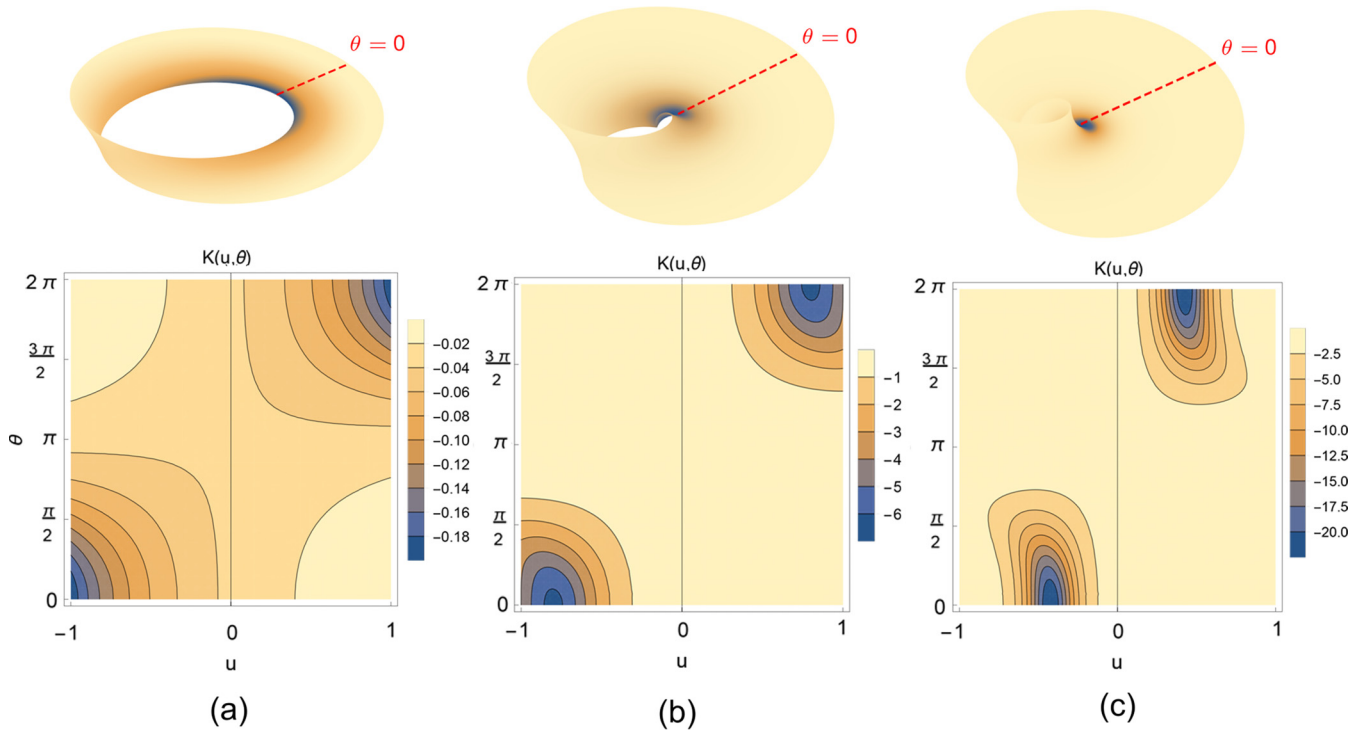


FIG. 3. Gaussian curvature on the Möbius strip, with $L/a = 0.375$ (a), $L/a = 1$ (b), and $L/a = 1.89$ (c), showing how the curvature is intrinsically distributed over the surface.

In Eq. (13), the gamma matrices on the surface γ^μ are defined as

$$\gamma^\mu = e_a^\mu \gamma^a, \tag{14}$$

where e_a^μ are the dreibeins. The spinorial covariant derivative D_μ is defined as

$$D_\mu = \partial_\mu - \Gamma_\mu, \tag{15}$$

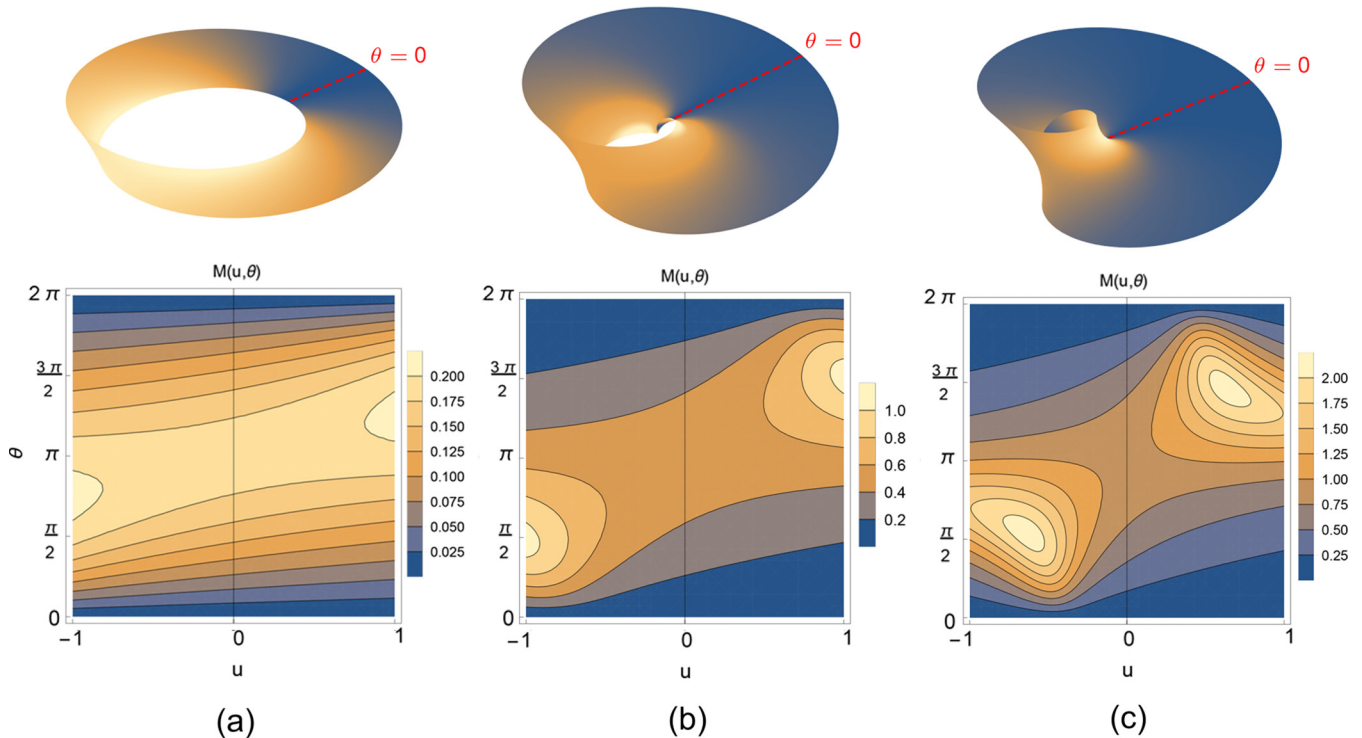


FIG. 4. Mean curvature on the Möbius strip with $L/a = 0.375$ (a), $L/a = 1$ (b), and $L/a = 1.89$ (c), showing how the curvature is extrinsically distributed over the surface.

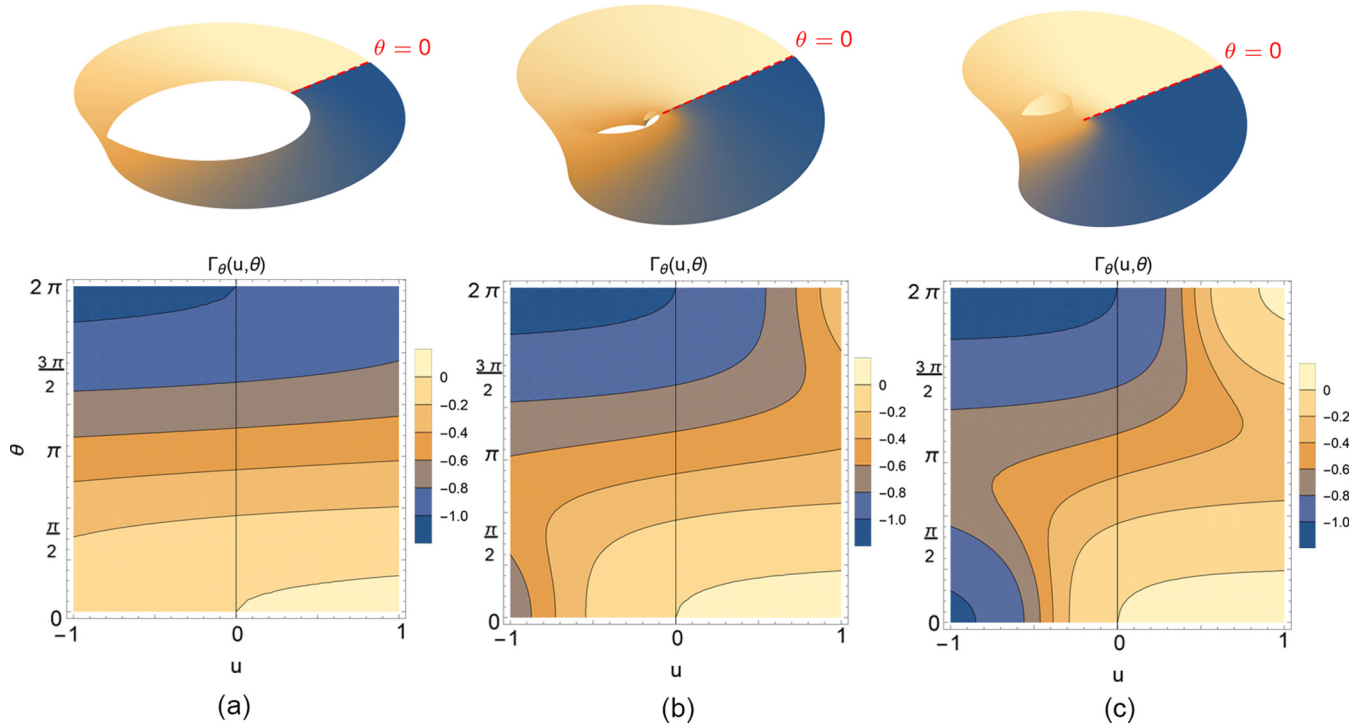


FIG. 5. Spinorial connection on the graphene Möbius strip with $L/a = 0.375$ (a), $L/a = 1$ (b), and $L/a = 1.89$ (c).

where the spinorial connection Γ_μ is defined as

$$\Gamma_\mu = \frac{1}{4} \omega_\mu^{ab} \gamma_a \gamma_b. \quad (16)$$

Since the curved covariant derivative in Eq. (15) is similar to the minimal coupling between an electron and a magnetic vector A_μ , the spinorial connection can be interpreted as a pseudomagnetic-potential vector induced by the curved geometry. In the spinorial connection in Eq. (16), ω_μ^{ab} are the connection 1-form and γ_a are the flat Dirac matrices. In this work we use the following representation of the Dirac matrices $\gamma^0 = -i\sigma_3$, $\gamma^1 = -\sigma_2$, and $\gamma^2 = \sigma_1$ [27].

From Eq. (12), since $\omega_2^1 = -(\partial_u \beta - 1)d\theta$, the only non-vanishing component of the spinorial connection is given by

$$\Gamma_\theta = -\frac{i}{2}(\partial_u \beta - 1)\sigma_3. \quad (17)$$

Thus, the pseudomagnetic potential has only one component along the angular direction. Incidentally, the corresponding pseudomagnetic field should point into the normal direction and it should be proportional to the Gaussian curvature [13].

The behavior of the spinorial connection along the graphene Möbius strip is shown in Fig. 5. We adopt the same values for the ratio L/a as done before, i.e., $L/a = 0.375$ (a), $L/a = 1$ (b), and $L/a = 1.89$ (c). Note that the spinorial connection profile is rather different from the Gaussian and mean curvatures. Indeed, the connection is greater for inner points ($u < 0$) than for outer points ($u > 0$) of the strip. For the sake of comparison, the spinorial connection for a cone is constant $\Gamma_\theta = -\frac{i}{2}(\alpha - 1)\sigma_3$ [23] and it vanishes for single-layer graphene, where $\alpha = 1$.

Hamiltonian

Let us consider a stationary electronic state, i.e.,

$$\psi(\mathbf{r}, t) = e^{\frac{iEt}{\hbar}} \varphi(\mathbf{r}). \quad (18)$$

Thus, the Dirac equation (13) reads

$$H\varphi = E\varphi, \quad (19)$$

where H is the stationary Hamiltonian of the relativistic electron at the graphene Möbius strip of the form

$$H = -i\hbar v_F \left[\sigma^1 \left(\partial_u - \frac{1}{2} \frac{(\partial_u \beta - 1)}{\beta} \right) + \frac{\sigma^2}{\beta} \partial_\theta \right]. \quad (20)$$

Using the Hermiticity relations of Dirac matrices, $(\gamma^i)^\dagger = \gamma^0 \gamma^i \gamma^0$, it is possible to show that the Hamiltonian in Eq. (20) is indeed Hermitian. In matrix notation, the Dirac equation in terms of the spinors is

$$-i \begin{pmatrix} 0 & \partial_u - \frac{i}{\beta} \partial_\theta - \frac{(\partial_u \beta - 1)}{2\beta} \\ \partial_u + \frac{i}{\beta} \partial_\theta - \frac{(\partial_u \beta - 1)}{2\beta} & 0 \end{pmatrix} \begin{pmatrix} \varphi_1 \\ \varphi_2 \end{pmatrix} = k \begin{pmatrix} \varphi_1 \\ \varphi_2 \end{pmatrix}, \quad (21)$$

where $\varphi_{1,2}(\mathbf{r}) = \varphi_{1,2}(u, \theta)$ and $k = \frac{E}{\hbar v_F}$ is the wave-vector norm (momentum).

It is worthwhile to mention that in the Hamiltonian Eq. (21) there is a geometric potential U_g of the form

$$U_g = -\frac{1}{2} \sigma^1 \frac{(\partial_u \beta - 1)}{\beta}. \quad (22)$$

The geometric potential U_g has a natural dimension of L^{-1} and it stems from the coupling between the fermion and the

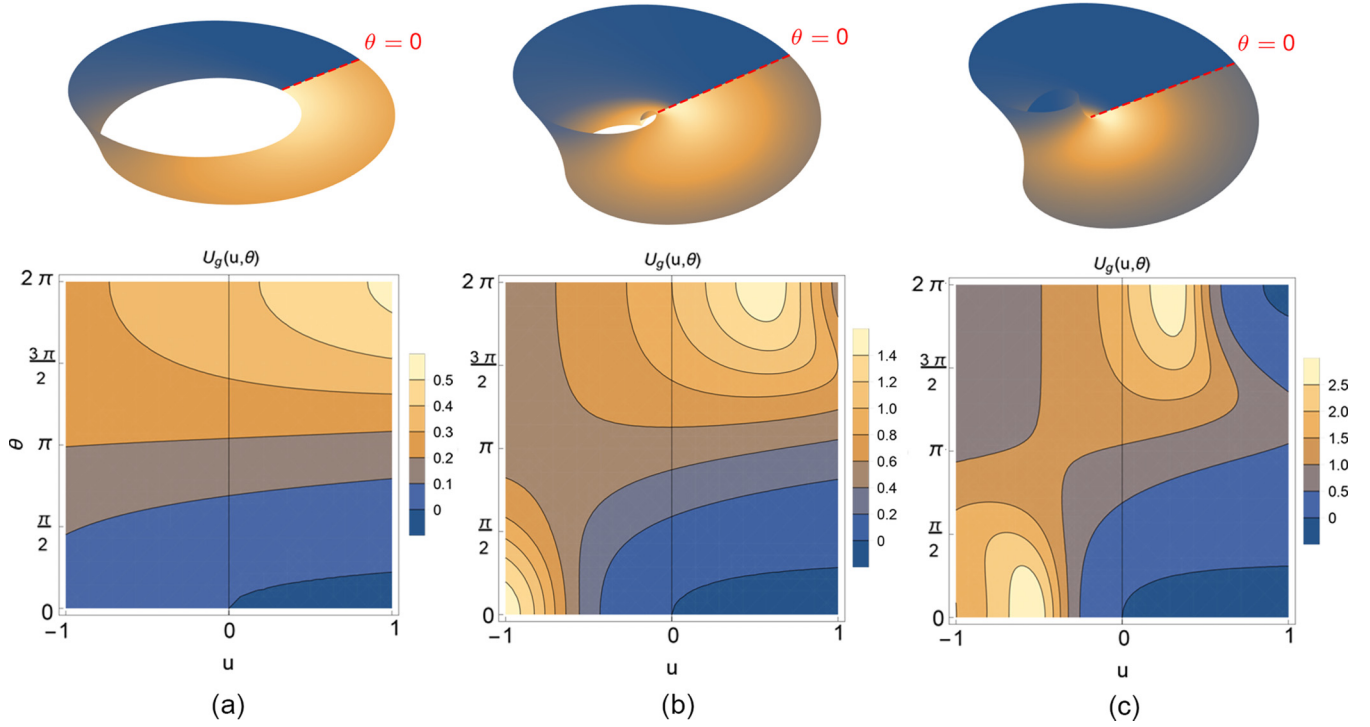


FIG. 6. Geometric potential U_g on the Möbius strip with $L/a = 0.375$ (a), $L/a = 1$ (b), and $L/a = 1.89$ (c).

spinorial connection. Note that for a conical surface, $U_g \approx \frac{(\alpha-1)}{u}$ [23], and thus, the geometric potential vanishes for a flat single-layer graphene sheet. We plotted the geometric potential for $L = 1$ in Fig. 6, where $L/a = 0.375$ (a), $L/a = 1$ (b), and $L/a = 1.89$ (c). The geometric potential has regions with positive and negative values near each other. Moreover, the potential exhibits a sort of Möbius modified parity symmetry of the form $(u, \theta) \rightarrow (-u, 2\pi - \theta)$.

Another noteworthy feature of the Hamiltonian in Eq. (21) is that it is no longer possible to write the wave function as $\varphi(u, \theta) = e^{i\ell\theta} \phi(u)$, as done for other surfaces such as the cone [23], helicoid [24], catenoid [26,27], and torus [28]. The reason for that stems from the lack of axial symmetry of the Möbius strip, which leads to a nonconservation of the angular momentum along the z axis [46]. As a result, no centrifugal term of the form $\frac{l}{\beta}$ arises naturally in the Hamiltonian Eq. (21).

IV. DIRAC FERMION ON WIRES

In the last section we described how the electron dynamics is modified by the curved geometry of the graphene Möbius strip. In this section we explore the electronic properties of the Dirac fermion constrained to wires along the graphene Möbius strip. By doing so, the fermion dynamics is dependent not only on the wire curvature but on the geometric potential U_g as well.

A. Wires along the width

Let us start with a wire directed along the strip width. In order to do it, we consider a given angle $\theta = \theta_0$ and vary the Hamiltonian in Eq. (21) only along the u direction. Since the

Hamiltonian is highly dependent on the angular coordinate θ , we investigate how the electron properties change as we consider different directions on the strip.

Along the u direction, we use $\beta = \beta(u, \theta_0)$ and $\partial_u \beta = \frac{\partial \beta(u, \theta)}{\partial u} |_{\theta=\theta_0}$. The Dirac equation Eq. (21) yields

$$\left(\partial_u - \frac{(1 - \partial_u \beta)}{2\beta} \right) \left(\partial_u - \frac{(1 - \partial_u \beta)}{2\beta} \right) \varphi_i = -k^2 \varphi_i, \quad (23)$$

where i can take on values 1 or 2. This equation, valid for both components of the spinor, can be rewritten as

$$\begin{aligned} \partial_u^2 \varphi_i - \left(\frac{(1 - \partial_u \beta)}{\beta} \right) \partial_u \varphi_i \\ + \left[\left(\frac{(1 - \partial_u \beta)}{2\beta} \right)^2 - \partial_u \left(\frac{(1 - \partial_u \beta)}{2\beta} \right) + k^2 \right] \varphi_i = 0, \end{aligned} \quad (24)$$

where the components of the spinor are decoupled and they satisfy the same Eq. (24).

Equation (24) can be further simplified by considering the change on the wave function

$$\varphi_i(u) = e^{-\frac{1}{2} \int \frac{(1 - \partial_u \beta)}{\beta} du} \chi_i(u), \quad (25)$$

where the new wave function $\chi_i(u)$ satisfies

$$-\frac{d^2 \chi_i(u)}{du^2} = k^2 \chi_i(u). \quad (26)$$

Accordingly, the exact wave function along the wire for (u, θ_0) is given by

$$\varphi_i(u, \theta_0) = \sqrt{\beta(u, \theta_0)} e^{(-\frac{1}{2} \int \frac{1}{\beta} du)} [A \cos(ku) + B \sin(ku)]. \quad (27)$$

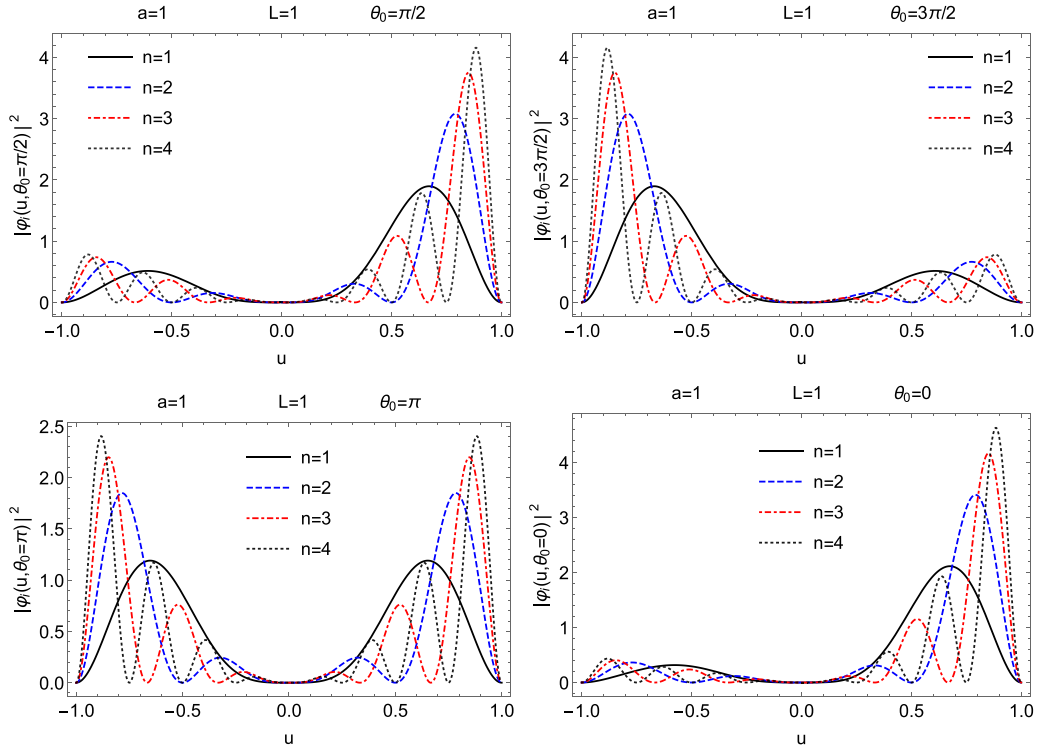


FIG. 7. Density of states along the width for θ_0 fixed. It shows the effect of the geometric phase concentrating the wave function at the outer region of the strip, leading to the formation of edge states.

Since the factor in the brackets is the solution for a free particle constrained inside the range $-L \leq u \leq L$, the effect of the Möbius geometry on the electron constrained to a wire along the width is encoded in the geometric phase

$$\Delta\phi = e^{-\frac{1}{2} \int \frac{(1-\partial_u\beta)}{\beta} du}. \quad (28)$$

It is worthwhile to mention that this geometric phase stems from the geometric potential U_g in Eq. (22) which depends on the connection rather than on the surface curvature. In a cylindrical surface (nanotubes), $\partial_u\beta = 0$ and the geometric phase is constant. On the other hand, for a flat plane (single-layer graphene), $\beta^2 = u^2$ and thus, the geometric phase vanishes identically.

Imposing the boundary conditions

$$\varphi_i(u = L, \theta_0) = \varphi_i(u = -L, \theta_0) = 0, \quad (29)$$

one obtains

$$A = 0 \quad \text{and} \quad \sin(kL) = 0, \quad (30)$$

for which the allowed energy spectrum is given by

$$E_n = n \frac{\pi}{L} \hbar v_F. \quad (31)$$

Note that the energy spectrum increases as the strip width L decreases. Moreover, the energy levels grow linearly with n and $\hbar v_F$, as expected from the Dirac equation. In Ref. [46], the authors found the energy spectrum for a nonrelativistic electron in the Möbius band is proportional to n^2 , an expected result stemming from the Schrödinger equation. In addition, the energy levels found in Eq. (31) are similar to the spectrum in a cylindrical ring. Indeed, since the geometric potential effects are encoded into the phase, the spectrum is the same

for a flat surface. For a ring with the same width as the one studied in Ref. [51], i.e., for $2L = 150$ nm, a typical electron with Fermi velocity $v_F = c/300$ has a ground state energy of about $E_0 \approx 2.75 \times 10^{-2}$ eV.

Therefore, the wave function along the wire is given by

$$\varphi_1(u, \theta_0) = C \sqrt{\beta(u, \theta_0)} e^{(-\frac{1}{2} \int \frac{1}{\beta} du)} \sin\left(\frac{n\pi u}{L}\right). \quad (32)$$

The effect of the geometric phase on the electron is shown in the Fig. 7, where we plotted the probability density $\varphi(u, \theta_0)\bar{\varphi}(u, \theta_0)$ for the four first energy levels. It is worthwhile to mention that the region where the fermion is localized on the wire depends on which angle θ_0 the wire is on the strip. Indeed, for $\theta_0 = \frac{\pi}{2}$, the wave function is concentrated at the outer region of the strip, whereas for $\theta_0 = \frac{3\pi}{2}$, the fermion is more localized at the inner region. Thus, the angle θ_0 can be understood as a parameter to tune the region where the electron is more concentrated. Moreover, note that the probability density does not possess parity symmetry for $\theta_0 = \{0, \pi/2, 3\pi/2\}$.

Another noteworthy feature shown in Fig. 7 is that the geometric phase tends to a damping of the amplitude of the Dirac fermion. In fact, by comparing the graphics of the wave function and the geometric potential, we can see that the fermion is more concentrated in the regions where the potential is less strong.

In Fig. 8, we plot the density of states on the Möbius strip for $n = 1$. We vary the ratio a/L for $L/a = 0.375$ (a), $L/a = 1$ (b) and $L/a = 1.89$, where we can see the formation of edge states. The presence of robust edge states has already been pointed out in Ref. [37], where the topological insulator

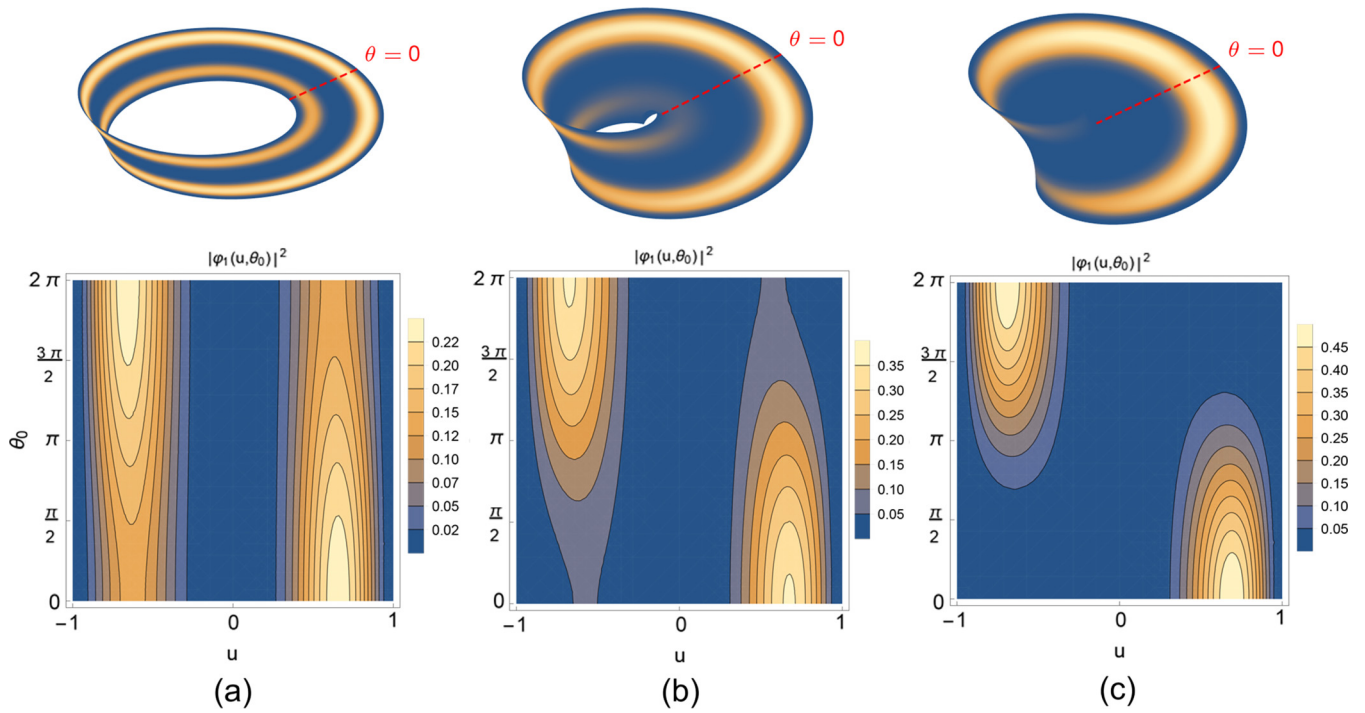


FIG. 8. Density of states along the Möbius surface for $n = 1$ with $L/a = 0.375$ (a), $L/a = 1$ (b), and $L/a = 1.89$ (c). The electron is more concentrated around the edges of the strip.

behavior of the Möbius strip was investigated. Moreover, note that the ground state ($n = 1$) in Fig. 8 exhibits only one ring state whereas the excited state for ($n = 4$) in Fig. 9 shows more ring states.

B. Wire along the strip length

Let us now consider the Dirac fermion constrained in a wire for a fixed $u = u_0$. For this case, we have no momentum along u , so that $\partial_u \psi = 0$. Also, $\beta = \beta(u_0, \theta)$ and

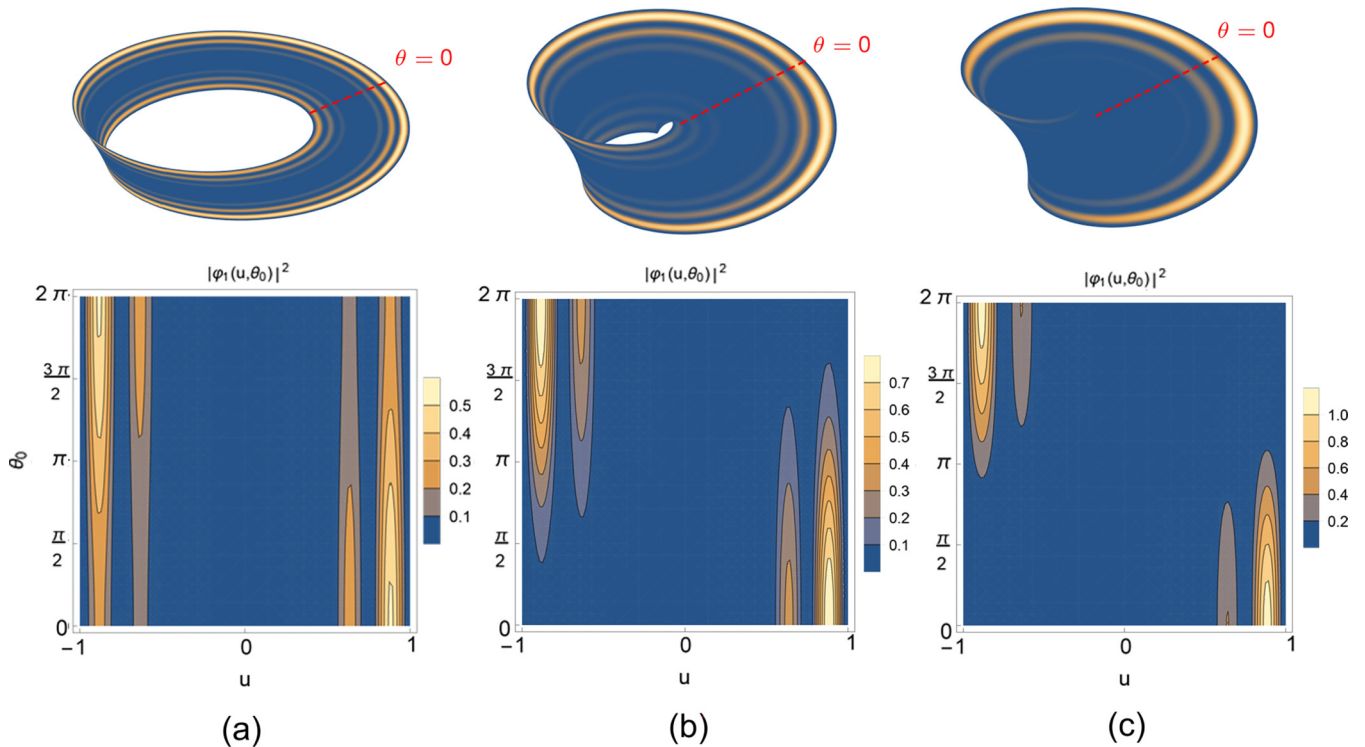


FIG. 9. Density of states along the Möbius surface for $n = 4$ with $L/a = 0.375$ (a), $L/a = 1$ (b), and $L/a = 1.89$ (c). Note the formation of more rings near the edges of the strip.

$\partial_u \beta = \frac{\partial \beta(u, \theta)}{\partial u} |_{u=u_0}$. Thus, by applying the Hamiltonian (20) to the wave function ψ , we obtain

$$H\psi = -i\hbar v_F \left[-\frac{1}{2} \frac{(\partial_u \beta - 1)}{\beta} \sigma^1 + \frac{\sigma^2}{\beta} \partial_\theta \right] \psi. \quad (33)$$

By making the change in the wave function

$$\psi(\theta, u_0) = e^{\Gamma_{\mu^{\lambda\mu}}} \psi_0 = e^{-\frac{i}{2} \frac{(\partial_u \beta - 1)}{\beta} \sigma^3} \psi_0(\theta, u_0), \quad (34)$$

we can simplify Eq. (33) to

$$H\psi_0 = -i\hbar v_F \frac{\sigma^2}{\beta} \partial_\theta \psi_0. \quad (35)$$

Thus, the Dirac equation $H\psi_0 = E\psi_0$ for the spinor ψ_0 whose components are of form

$$\psi_0 = \begin{pmatrix} \Phi_1(\theta) \\ \Phi_2(\theta) \end{pmatrix} \quad (36)$$

yields to the system

$$-i \begin{pmatrix} 0 & -\frac{i}{\beta} \partial_\theta \\ \frac{i}{\beta} \partial_\theta & 0 \end{pmatrix} \begin{pmatrix} \Phi_1 \\ \Phi_2 \end{pmatrix} = k \begin{pmatrix} \Phi_1 \\ \Phi_2 \end{pmatrix}, \quad (37)$$

where $k = \frac{E}{\hbar v_F}$. By decoupling the system in Eq. (37) leads us to a differential equations valid for both components of the spinor given by

$$-\frac{1}{\beta} \frac{d}{d\theta} \left(\frac{1}{\beta} \frac{d\Phi_i}{d\theta} \right) = k^2 \Phi_i(\theta). \quad (38)$$

Equation (38) can be further simplified by considering the change of coordinate

$$v(\theta) = \int_0^\theta \beta(u_0, \theta') d\theta', \quad (39)$$

where $dv = \beta(u_0, \theta) d\theta$ is the infinitesimal arclength. Accordingly, the decoupled Dirac equation (38) reads

$$\frac{d^2 \Phi_i(v)}{dv^2} + k^2 \Phi_i(v) = 0, \quad (40)$$

whose exact solutions for the components of the spinor ψ along the strip length are given by

$$\begin{aligned} \varphi_1(\theta) &= e^{iW(\theta)} \left[A \cos \left(k \int_0^\theta \beta(u_0, \theta') d\theta' \right) \right. \\ &\quad \left. + B \sin \left(k \int_0^\theta \beta(u_0, \theta') d\theta' \right) \right], \\ \varphi_2(\theta) &= e^{-iW(\theta)} \left[C \cos \left(k \int_0^\theta \beta(u_0, \theta') d\theta' \right) \right. \\ &\quad \left. + D \sin \left(k \int_0^\theta \beta(u_0, \theta') d\theta' \right) \right], \end{aligned} \quad (41)$$

where the geometric phase $W(\theta)$ along the angular wire is given by

$$W(\theta) = -\frac{1}{2} \frac{(\partial_u \beta - 1)}{\beta}. \quad (42)$$

It is worthwhile to mention that, despite that the geometric phase $e^{iW(\theta)}$ modifies the wave function, the probability distribution $\varphi\bar{\varphi}$ is independent of W . This is key feature of the

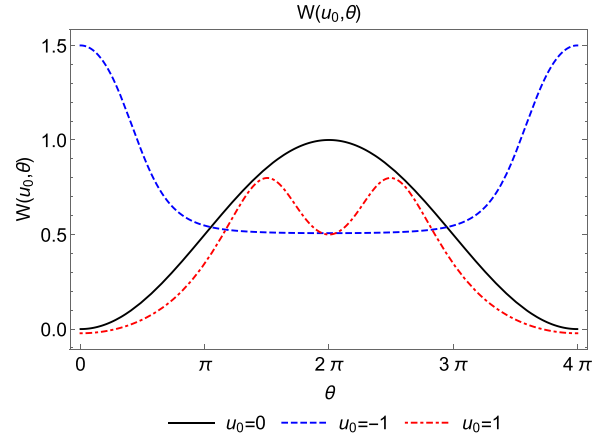


FIG. 10. Geometric phase along the θ direction for $u_0 = 0, \pm 1$ showing its 4π periodic behavior.

geometric phases [23], and a similar property is also shared with the Aharonov-Bohm phase [51].

Another noteworthy result is related to the period of the wave function. Indeed, by Eq. (41) the period strongly depends on the metric function $\beta(u_0, \theta)$. Thus, let us now investigate the effects of the geometry of the angular wires on the electronic states.

1. Central ring

At the center of the strip, i.e., for $u = 0$, the wire forms a closed ring. The angular metric factor β takes the form

$$\beta(u_0 = 0, \theta) = a, \quad (43)$$

and thus, the metric on this ring is independent of θ . As a result, the geometric phase has the form

$$W(\theta) = \frac{1}{2} \left[1 - \cos \left(\frac{\theta}{2} \right) \right], \quad (44)$$

and the first spinor component wave function is given by

$$\varphi_1(\theta) = e^{i\frac{1}{2}[1 - \cos(\frac{\theta}{2})]} [A \cos ka\theta + B \sin ka\theta]. \quad (45)$$

The second spinor component wave function can be obtained from Eq. (45) by making $W \rightarrow -W$. Interestingly, although the wire for $u = 0$ forms a circular ring, the Möbius strip still induces an anisotropic geometric phase. This result shows the difference between an usual ring and one constrained on the Möbius surface.

Even though the geometric phase $W(\theta)$ is a 4π periodic function, as shown in Fig. 10, the period of the wave function is determined by the trigonometric function inside the brackets. In fact, by considering the periodic boundary conditions

$$\varphi_1(0, \theta = 0) = \varphi_1(0, \theta = 2\pi) = 0, \quad (46)$$

the wave function has the form

$$\varphi_1(\theta) = A e^{iW(\theta)} \sin(ak\theta). \quad (47)$$

Since $e^{iW(\theta)}$ lies at the unit circle in the complex plane, this factor never vanishes. Thus, the wave function period is determined by the $\sin ka\theta$ function.

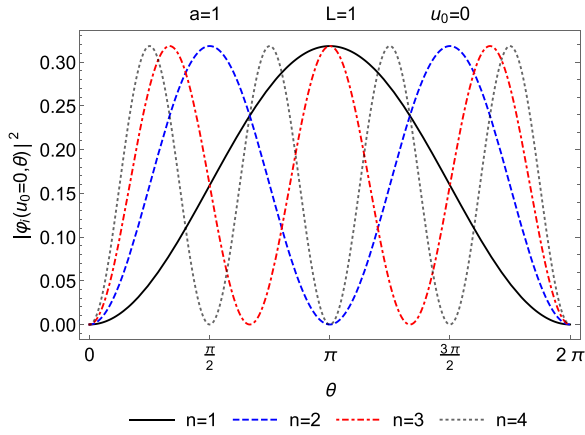


FIG. 11. Density of states at the central ring ($u = 0$) for the initial four energy levels. The wave function shows a free particle behavior, since in this case the geometric phase does not affect the density probability.

Using the boundary condition on the central ring in Eq. (46), the momentum is given by

$$k_n = \frac{n}{2a}, \quad (48)$$

and thus, the wave function has the form

$$\varphi_1(\theta) = A e^{iW(\theta)} \sin\left(n\frac{\theta}{2}\right), \quad (49)$$

where n is a integer number. It is worthwhile to mention that the ground state ($n = 1$) has a period of 4π , whereas the first excited state ($n = 2$) is a 2π periodic function. For the n th state, the period is $T_n = 4\pi/n$, and hence for n odd, the period is a noninteger multiple of 4π . This feature results from the Möbius strip geometry and similar results were found for a nonrelativistic electron [46].

In Fig. 11 we plotted the probability density $\psi\bar{\psi}$ for the first electronic states. The figure shows that the ground state ($n = 1$) is centered at $\theta = \pi$, whereas the first excited state ($n = 2$) has two peaks symmetrically displaced from $\theta = \pi$. As n increases, the number of peaks increases as well. Besides, for odd n the probability density has a peak at $\theta = \pi$, whereas for even n the probability vanishes at this point.

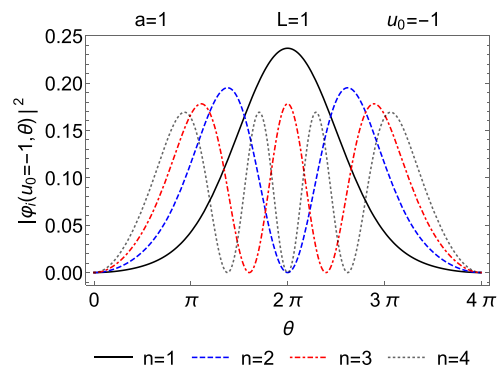
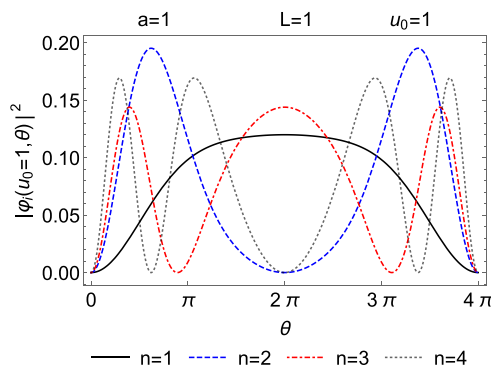


FIG. 12. Density of states at the edge wires ($u = \pm 1$) for the initial four energy levels.

Accordingly, the allowed energies E_n are given by

$$E_n = \frac{n \hbar v_F}{2a}. \quad (50)$$

Note that the energy decreases as the inner radius a increases, as expected for a usual ring. Furthermore, it is important to mention that the spectrum is the same for both components of the spinor. However, the nontrivial topology leads to an energy spectrum which is the half-integer multiple of the ground state, shown in Eq. (50). A similar result for a nonrelativistic electron was found in Ref. [46]. For a ring with the same inner radius as the one studied in Ref. [51], i.e., for $a = 200$ nm, the energy of the ground state is $E_0 \approx 1.64 \times 10^{-3}$ eV, which is lower than the ground state energy for a wire along the width. It is worthwhile to mention that the values $a = 200$ nm and $L = 75$ nm lead to the ratio $L/a = 0.375$ and thus, they can be used to form a stable Möbius strip [39].

2. Edge wires

For wires at the edge of the Möbius band, i.e., for $u = \pm 1$, the wires do not form closed rings. The arclength variable v for the outer edge is given by

$$v(\theta)|_{u=1} = \int_0^\theta \left[\frac{1}{4} + [1 + \cos(\theta'/2)]^2 \right]^{1/2} d\theta', \quad (51)$$

whereas for the inner edge it has the form

$$v(\theta)|_{u=-1} = \int_0^\theta \left[\frac{1}{4} + [1 - \cos(\theta'/2)]^2 \right]^{1/2} d\theta', \quad (52)$$

where we assume that $-1 \leq u \leq 1$. Since the $\beta(\pm 1, \theta)$ is periodic with period 4π , then $v(\theta)$ is also a 4π periodic function. Therefore, the wave function has the form

$$\varphi_1(\theta) = e^{iW(\theta)} \{A \cos[kv(\theta)] + B \sin[kv(\theta)]\}. \quad (53)$$

Since $v(0) = 0$, using the boundary conditions, the wave function is given by

$$\varphi_1(\theta) = A e^{iW(\theta)} \sin[k_n v(\theta)], \quad (54)$$

where k_n satisfies the condition

$$k_n \int_0^{4\pi} \beta(u_0, \theta) d\theta = n\pi. \quad (55)$$

We plot the probability densities in Fig. 12. Note that the probability associated with the ground state is concentrated

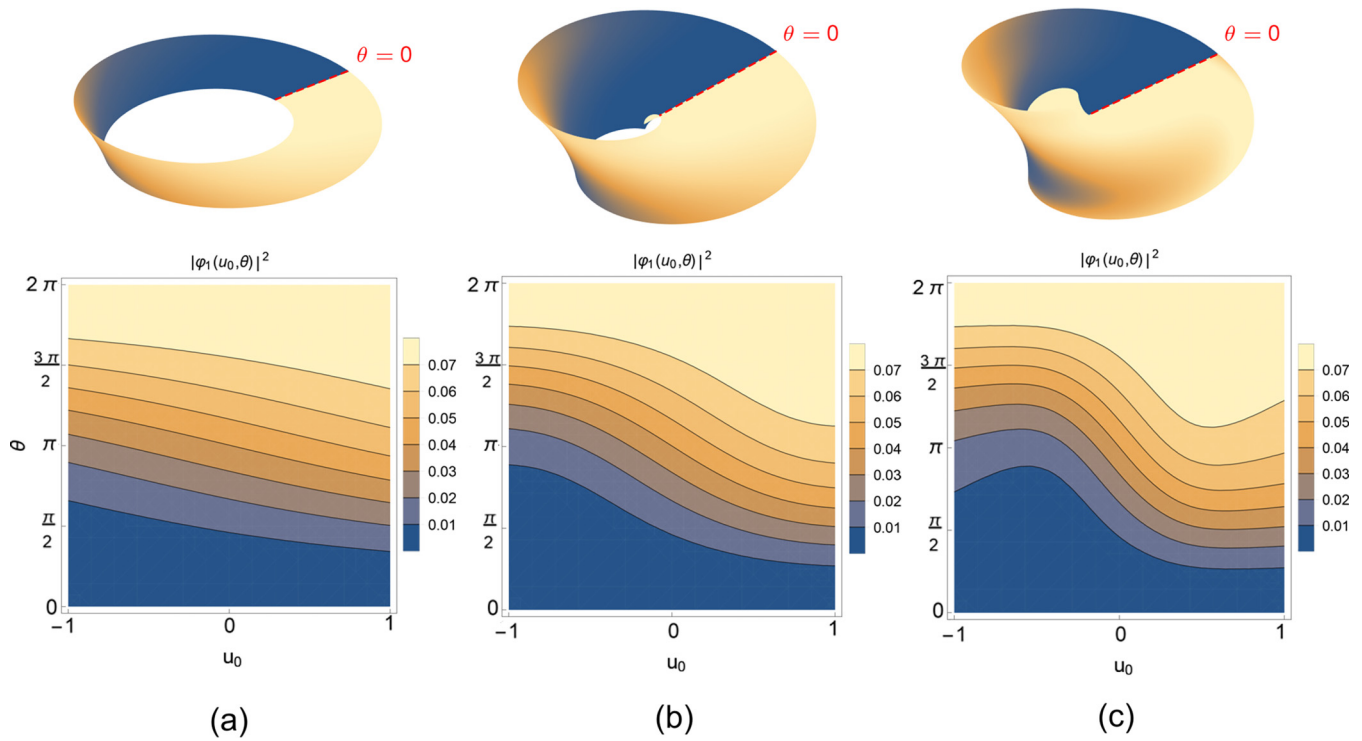


FIG. 13. Density of states along the Möbius strip for $n = 1$ with $L/a = 0.375$ (a), $L/a = 1$ (b), and $L/a = 1.89$ (c).

at $\theta = 2\pi$ for $u = -1$ and $u = 1$. Moreover, the first excited state has two peaks shifted from the point 2π . As n increases, the number of peaks also increases. Besides, the pattern of the wave functions for even n differs from those for odd n .

Figure 13 shows how the density of states is distributed on the Möbius strip for $n = 1$. Note that the ground state (upper graphics) resembles the geometric potential profile shown in Fig. 6. For $n = 4$, shown in Fig. 14, note that the density of states is rather dependent on the ratio a/L .

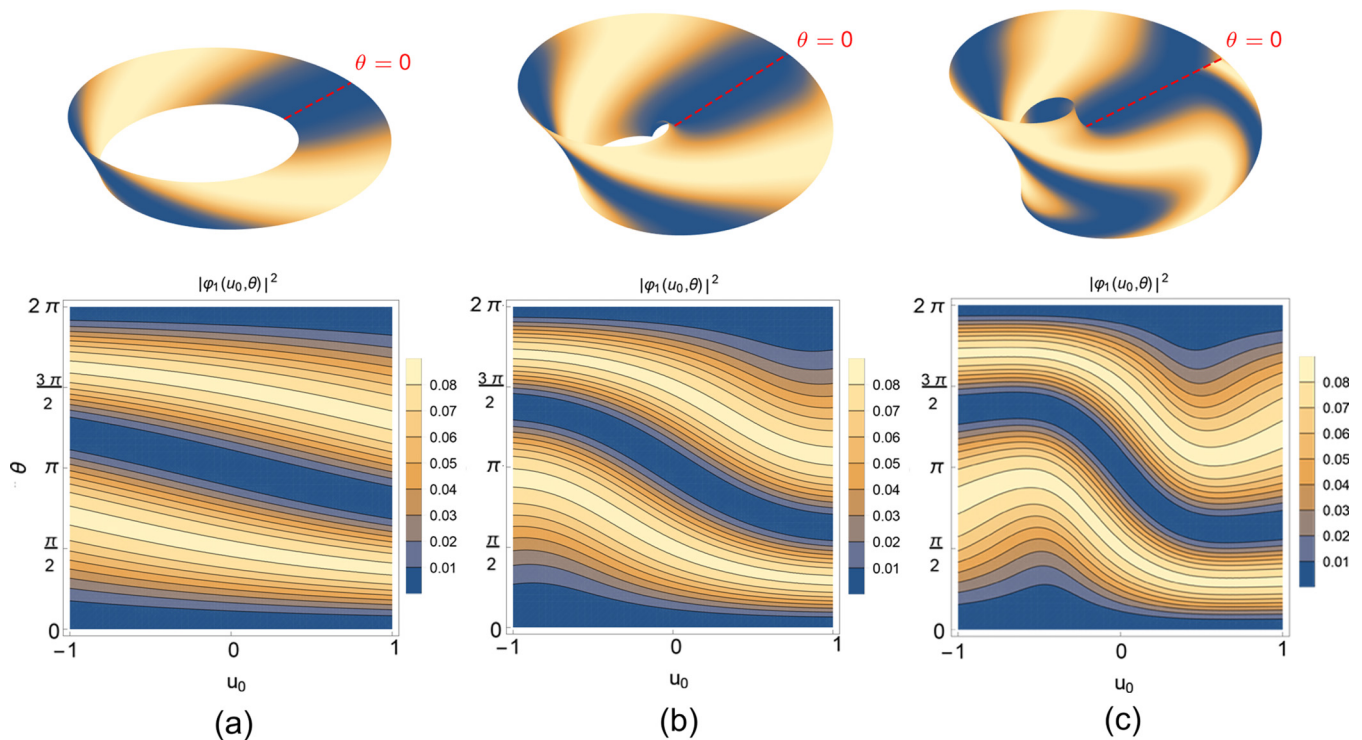


FIG. 14. Density of states along the Möbius strip for $n = 4$ with $L/a = 0.375$ (a), $L/a = 1$ (b), and $L/a = 1.89$ (c).

V. DISCUSSION AND PERSPECTIVES

In this work we found exact solutions for an electron constrained to wires along a graphene Möbius strip. Such a surface can be formed by performing a twist on one graphene ribbon end and connecting it to the another end. By considering the electron effectively described as a massless Dirac fermion, the Möbius strip curved geometry provides a geometric potential depending on the geometric connection instead of the curvature. The geometry of the wires depends not only on the wire metric but on the Möbius geometry and symmetries, as well.

For wires along the strip width, i.e., for a given θ_0 , the effects of the curved geometry are encoded into a geometric phase which stems from the geometric potential. As a result, exact solutions for the Dirac equation were found which shows the formation of edge states. As we increase the energy, additional edge states forming rings appear. Moreover, the electronic probability density is highly dependent on the direction θ_0 chosen for the wire. In fact, for some θ_0 the electron is more concentrated near the inner edge, whereas for other values of θ_0 the wave function is localized toward the outer edge of the band. This behavior agrees with the lack of parity symmetry of the Möbius band, i.e., $\beta(-u, \theta_0) \neq \beta(u, \theta_0)$.

On the other hand, the wires along the strip length have a rather different geometry from those along the width. For $u = 0$, the wire forms a ring of radius a , whereas for $u = \pm L$ (strip edges) the wire is open in the interval $0 \leq \theta \leq 2\pi$. Due to the Möbius strip geometry, the wires for $u_0 \neq 0$ are actually close if we consider the period 4π . Accordingly, we expect the wave function to be a periodic function of period 4π . It turns out that, for the central ring at $u = 0$, the ground state is a 4π periodic function whose probability density is localized around $\theta = \pi$. For n odd, the wave function has a period that is a noninteger multiple of 2π . Similarly, the energy levels are half-integer multiples of the quantum $\hbar v_F/a$. These noninteger features of both the electronic states and the spectrum are the result of the nontrivial geometry of the Möbius band. For a ring with the same inner radius as the cylindrical ring studied in Ref. [51], i.e., for $a = 200$ nm, the energy of the ground state is $E_0 \approx 1.64 \times 10^{-3}$ eV. Since the ratio $L/a = 0.375$ is smaller than the critical ratio, the nontrivial topology of the Möbius strip could be used to generate a geometric Aharonov-Bohm effect due to pseudomagnetic field.

For the wires along the edges of the Möbius strip, the ground states $n = 1$ exhibit a localized probability density around $\theta = 2\pi$. Once again, the break of the parity symmetry

yields to a different profile between the ground state at the inner edge ($u_0 = -L$) and at the outer edge ($u_0 = L$). The electronic states for the outer edge are more concentrated than those at the inner edge.

A remarkable result we found is the role played by the geometric phase on the electronic states. For the wires along the width, the Dirac equation can be simplified by considering a geometric phase depending on the geometric potential. It turns out that the energy levels and the period of the electronic states are determined as if the strip were flat. A similar result was found numerically by Ref. [46], though the authors considered a nonrelativistic electron. On the other hand, the geometric phase provides a damping of the wave function, which leads to the parity-breaking profile discussed above. Along the angular direction, the geometric phase is given by the geometric (spinor) connection. Likewise, for the well-known Aharonov-Bohm phase, the geometric phase does not alter the density of states for a single electron. Hence, the period of the electronic states and the energy levels are determined by the angular metric function along the wire, i.e., $\beta(u_0, \theta)$. This shows that the electronic properties on wires along the Möbius strip are different from those in the usual circular wires, for the wires inherit the anisotropic Möbius geometry.

This work suggests as a perspective the investigation of the effects of the geometric phase on the interference pattern between electrons. Indeed, Aharonov-Bohm effects on graphene-gated cylindrical nanorings of width $L = 75$ nm and inner radius $a = 200$ nm ($L/a = 0.375$) were investigated [51]. By considering a Möbius ring with the same size, similar effects could be observed due to the geometric phase. Moreover, the inclusion of external fields might lead to an additional parameter to control the density of states. In addition, the interaction of the confined electron to the external electric or magnetic fields should leave a peculiar signature which could be used to characterize the material. In fact, as proposed in Ref. [13] transmission electron microscopy (TEM) or scanning tunneling microscopy (STM) can be used to probe the morphology and relate it to the density of states. For the Möbius graphene strip, these microscopic techniques could be used to determine the ratio L/a of the samples.

ACKNOWLEDGMENT

The authors thank the Conselho Nacional de Desenvolvimento Científico e Tecnológico (CNPq), Grants No. 312356/2017-0 (JEGS) and No. 309553/2021-0 (CASA), for financial support.

[1] A. K. Geim and K. S. Novoselov, *Nat. Mater.* **6**, 183 (2007).
 [2] A. K. Geim, *Science* **324**, 1530 (2009).
 [3] K. S. Novoselov, K. Geim, V. Morozov, D. Jiangy, Y. Zhangs, S. V. Dubonos, V. Grigorieva, and A. A. Firsov, *Science* **306**, 666 (2004).
 [4] A. H. Castro Neto, F. Guinea, N. M. R. Peres, K. S. Novoselov, and A. K. Geim, *Rev. Mod. Phys.* **81**, 109 (2009).
 [5] M. I. Katsnelson, *Graphene: Carbon in Two Dimensions* (Cambridge University Press, Cambridge, UK, 2012).
 [6] M. I. Katsnelson, *Eur. Phys. J. B* **51**, 157 (2006).

[7] M. I. Katsnelson, K. S. Novoselov, and A. K. Geim, *Nat. Phys.* **2**, 620 (2006).
 [8] A. Cortijo, Y. Ferreirós, K. Landsteiner, and M. A. H. Vozmediano, *Phys. Rev. Lett.* **115**, 177202 (2015).
 [9] S. Rachel, L. Fritz, and M. Vojta, *Phys. Rev. Lett.* **116**, 167201 (2016).
 [10] E. M. Nica and M. Franz, *Phys. Rev. B* **97**, 024520 (2018).
 [11] T. Liu, *Phys. Rev. B* **102**, 045151 (2020).
 [12] V. M. Pereira, A. H. Castro Neto, H. Y. Liang, and L. Mahadevan, *Phys. Rev. Lett.* **105**, 156603 (2010).

- [13] F. de Juan, A. Cortijo, and M. A. H. Vozmediano, *Phys. Rev. B* **76**, 165409 (2007).
- [14] F. de Juan, M. Sturla, and M. A. H. Vozmediano, *Phys. Rev. Lett.* **108**, 227205 (2012).
- [15] M. A. H. Vozmediano, M. I. Katsnelson, and F. Guinea, *Phys. Rep.* **496**, 109 (2010).
- [16] F. de Juan, J. L. Mañes, and M. A. H. Vozmediano, *Phys. Rev. B* **87**, 165131 (2013).
- [17] P. Castro-Villarreal and R. Ruiz-Sánchez, *Phys. Rev. B* **95**, 125432 (2017).
- [18] T. Liu and Z. Shi, *Phys. Rev. B* **103**, 144420 (2021).
- [19] A. Fasolino, J. H. Los, and M. I. Katsnelson, *Nat. Mater.* **6**, 858 (2007).
- [20] F. Guinea, B. Horowitz, and P. Le Doussal, *Solid State Commun.* **149**, 1140 (2009).
- [21] V. Atanasov and A. Saxena, *Phys. Rev. B* **81**, 205409 (2010).
- [22] S. Deng and V. Berr, *Mater. Today* **19**, 197 (2016).
- [23] C. Furtado, F. Moraes, and A. M. de M. Carvalho, *Phys. Lett. A* **372**, 5368 (2008).
- [24] M. Watanabe, H. Komatsu, N. Tsuji, and H. Aoki, *Phys. Rev. B* **92**, 205425 (2015).
- [25] V. Atanasov and A. Saxena, *Phys. Rev. B* **92**, 035440 (2015).
- [26] J. E. G. Silva, J. Furtado, T. M. Santiago, A. C. A. Ramos, and D. R. Da Costa, *Phys. Lett. A* **384**, 126458 (2020).
- [27] Ö. Yeşiltaş, J. Furtado, and J. E. G. Silva, *Eur. Phys. J. Plus* **137**, 416 (2022).
- [28] J. E. G. Silva, J. Furtado, T. M. Santiago, and A. C. A. Ramos, *Eur. Phys. J. B* **93**, 225 (2020).
- [29] F. de Juan, A. Cortijo, M. A. H. Vozmediano, and A. Cano, *Nat. Phys.* **7**, 810 (2011).
- [30] S.-J. Choi, S. Park, and H.-S. Sim, *Phys. Rev. B* **89**, 155412 (2014).
- [31] A. Mesaros, D. Sadri, and J. Zaanen, *Phys. Rev. B* **79**, 155111 (2009).
- [32] P. E. Lammert and V. H. Crespi, *Phys. Rev. Lett.* **85**, 5190 (2000).
- [33] A. J. Chaves *et al.*, *J. Phys.: Condens. Matter* **26**, 185301 (2014).
- [34] N. Zhao, H. Dong, S. Yang, and C. P. Sun, *Phys. Rev. B* **79**, 014105 (2009).
- [35] M. Spivak, *A Comprehensive Introduction to Differential Geometry*, 3rd ed. (Publish or Perish, Inc., Boston, 1999), Vol. 3.
- [36] E. L. Starostin and G. H. M. van der Heijden, *J. Elast.* **119**, 67 (2015).
- [37] Z. L. Guo, Z. R. Gong, H. Dong, and C. P. Sun, *Phys. Rev. B* **80**, 195310 (2009).
- [38] D. J. Ballon and H. U. Voss, *Phys. Rev. Lett.* **101**, 247701 (2008).
- [39] X. Wang, X. Zheng, M. Ni, L. Zou, and Z. Zenga, *Appl. Phys. Lett.* **97**, 123103 (2010).
- [40] E. W. S. Caetano, V. N. Freire, S. G. dos Santos, D. S. Galvão, and F. Sato, *J. Chem. Phys.* **128**, 164719 (2008).
- [41] X. Zhang, B. Tian, W. Zhen, Z. Li, Y. Wu, and G. Lu, *J. Catal.* **354**, 258 (2017).
- [42] S. Yue, Q. Yan, Z. Zhu, H. Cui, Q. Zheng, and G. Su, *Carbon* **71**, 150 (2014).
- [43] A. Quelle, W. Beugeling, and C. Morais Smith, *Solid State Commun.* **215-216**, 27 (2015).
- [44] K. Flouris, M. M. Jimenez, and H. J. Herrmann, *Phys. Rev. B* **105**, 235122 (2022).
- [45] A. D. Güçlü, M. Grabowski, and P. Hawrylak, *Phys. Rev. B* **87**, 035435 (2013).
- [46] Z. Li and L. R. Ram-Mohan, *Phys. Rev. B* **85**, 195438 (2012).
- [47] J. F. O. de Souza and C. Furtado, *Int. J. Mod. Phys. B* **30**, 1650224 (2016).
- [48] M. Burgess and B. Jensen, *Phys. Rev. A* **48**, 1861 (1993).
- [49] B. Jensen and R. Dandoloff, *Phys. Lett. A* **375**, 448 (2011).
- [50] A. Cortijo and M. A. H. Vozmediano, *Europhys. Lett.* **77**, 47002 (2007).
- [51] P. Recher, B. Trauzettel, A. Rycerz, Ya. M. Blanter, C. W. J. Beenakker, and A. F. Morpurgo, *Phys. Rev. B* **76**, 235404 (2007).